Monitoring the three-dimensional distribution of endogenous species in the lungs by matrix-assisted laser desorption/ionization mass spectrometry imaging

FLINDERS, Bryn, MORRELL, Josie, MARSHALL, Peter S, RANSHAW, Lisa E, HEEREN, Ron MA and CLENCH, Malcolm <http://orcid.org/0000-0002-0798-831X>

Monitoring the three-dimensional distribution of endogenous species in the lungs by MALDI-MSI

Bryn Flinders [1,3†], Josie Morrell [2], Peter S. Marshall [2], Lisa E. Ranshaw [2], Ron M. A. Heeren[3], Malcolm R. Clench [1*]

[1.] Centre for Mass Spectrometry Imaging, Biomedical Research Centre, City Campus, Sheffield Hallam University, Sheffield, S1 1WB

[2.] GlaxoSmithKline, Gunnels Wood Road, Stevenage, Hertfordshire, SG1 2NY

[3.] Maastricht Multimodal Molecular Imaging Institute (M4I), Maastricht University, Universiteitssingel 50, 6229 ER, Maastricht, The Netherlands.

Bryn Flinders bryn.flinders@student.shu.ac.uk, Josie Morrell josie.l.morrell@gsk.com, Peter S. Marshall peter.s.marshall@gsk.com, Lisa E. Ranshaw lisa.e.ranshaw@gsk.com, Ron M. A. Heeren r.heeren@maastrichtuniversity.nl, Malcolm R. Clench m.r.clench@shu.ac.uk.

† Current address: Hair Diagnostix, Dutch Screening Group, Gaetano Martinolaan 63A, 6229 GS Maastricht, The Netherlands.

Corresponding author*: Prof. Malcolm Clench, tel +441142253054, fax +441142253064, email: m.r.clench@shu.ac.uk

Abstract

Rationale: Matrix-assisted laser desorption/ionization-mass spectrometry imaging (MALDI-MSI) is routinely employed to monitor the distribution of compounds in tissue sections and generate 2D images, whilst informative the images do not represent the distribution of the analyte of interest through the entire organ. The generation of 3D images is an exciting field that can provide a deeper view of the analyte of interest throughout an entire organ.

Methods: Serial sections of mouse and rat lung tissue were obtained at 120 µm depth intervals and imaged individually. Homogenate registration markers were incorporated in order to aid the final 3D image construction. Using freely available software packages, the images were stacked together to generate a 3D image that showed the distribution of endogenous species throughout the lungs.

Results: Preliminary tests were performed on 16 serial tissue sections of mouse lungs. A 3D model showing the distribution of phosphocholine at *m/z* 184.09 was constructed, which defined the external structure of the lungs and trachea. Later, a second experiment was performed using 24 serial tissue sections of the left lung of a rat. Two molecular markers, identified as $[PC\ (32:1)+K]^+$ at *m/z* 770.51 and $[PC\ (36:4)+K]^+$ at *m/z* 820.52 were used to generate 3D models of the parenchyma and airways respectively.

Conclusions: A straightforward method to generate 3D MALDI-MS images of selected molecules in lung tissue has been presented. Using freely available imaging software, the 3D distributions of molecules related to different anatomical features were determined.

Keywords:
MALDI-MSI, Image J, lungs, 3D, lipids.

Introduction

Imaging techniques such as computed tomography (CT), magnetic resonance imaging (MRI) and positron emission tomography (PET) are commonplace in modern medicine, they are routinely used to provide anatomical information for diagnosis of diseases such as cancer[1]. These techniques are capable of non-invasive three-dimensional (3D) imaging by generating several 2D images of an organ which are rendered into a 3D model. Combinations of these techniques such as CT-PET or MRI-PET can be used to provide more information by viewing the data from different modalities together in a 3D model[2]. However, these techniques are targeted and therefore provide limited molecular information.

Matrix-assisted laser desorption/ionization-mass spectrometry imaging (MALDI-MSI) has been extensively used to generate two-dimensional (2D) images showing the distribution of drugs, lipids peptides and proteins in tissue sections. However, this does not necessarily represent the distribution of a molecule throughout the entire organ. Expanding this technique with the addition of a third dimension would enable a detailed, volumetric visualization of these analytes in an entire organ could bridge the gap between molecular and medical imaging techniques.

There are currently two approaches used for generating 3D images with mass spectrometry imaging (MSI), depth profiling and serial-sectioning. In the depth profiling approach, ablation of the sample surface is performed exposing lower layers for analysis. This approach has been reported using secondary ion mass spectrometry (SIMS) to generate 3D images of single cells by monitoring the distribution of two endogenous species (adenine and phosphocholine) the nucleus and cell membrane could be visualized respectively[3]. Laser ablation electrospray ionization (LAESI) is also capable of this type of analysis and has been used to visualize various metabolites in the leaves of a zebra plant[4].

In order to visualize the distribution of molecules throughout an entire organ the serial-sectioning approach is used. In this approach, the sample is cut into serial sections and each section is imaged and then combined into a 3D model. This methodology has primarily been reported using matrix-assisted laser desorption/ionization (MALDI), the first report visualized the distribution of the myelin basic protein (MBP) in the corpus callosum of a mouse brain. The sample was sectioned into a total of 264 tissue sections from which 10 sections were selected at equal intervals and analyzed by MALDI-MSI. Optical images of all the sections were then used to create a 3D volume of the corpus callosum, the MALDI-MS images were then rendered into the 3D volume[5].

Mouse or rat brains are the most commonly used specimens to visualize due to their size and the availability of anatomical/histological references, which can be used to co-register with the MALDI-MS images. Later

examples monitored the 3D distribution of peptides and proteins in the substantia nigra and interpeduncular nucleus[6], proteins have also been visualized in a mouse brain tumor which were co-registered with MRI data[7], lipids associated with traumatic brain injury[8] and recently lipids in medulloblastoma metastasis[9]. The 3D distribution of peptides and lipids has even been visualized in a crab brain[10]. Ambient ionization techniques such as desorption electrospray ionization-mass spectrometry imaging (DESI-MSI) have also been used to investigate the 3D distribution of lipids that make up the white and grey matter in mouse brain[11]. 3D imaging has also been shown to be a useful technique to help better understand the molecular make-up of tumor tissue and to better define the boundaries between the different tissue types[12,13]. This is due to the heterogeneous nature of tumor tissue, which cannot be accurately represented in a single tissue section. The quantitative 3D imaging of chemotherapeutic agents in tumor tissue has also been demonstrated[14].

As the previous examples demonstrate 3D imaging with mass spectrometry imaging is becoming more widely applied due to its ability to help with complex tissues and to better understand diseases. This widespread application is also being facilitated by the development of faster commercial instruments and software[15,16].

The aim of the work reported here is to develop methodology to monitor the three-dimensional distribution of endogenous species throughout the lungs using MALDI-MSI. Serial sections were obtained at 120 µm depth-intervals through the control mouse lung tissue and imaged individually, homogenate registration markers were incorporated in order to aid the final 3D image construction using freely available software.

Methods

Information

Healthy mouse lung tissue was obtained from a control batch of tissue, however the strain could not be verified. All animal studies were ethically reviewed and carried out in accordance with UK Animals (Scientific Procedures) Act 1986, European Directive 2010/63/EU and the GSK Policy on the Care, Welfare and Treatment of Laboratory Animals. Healthy rat lung tissue (Wistar Han) was obtained from a control group of rats sacrificed for a study on colonic anastomotic healing. The experimental protocol compiled with the Dutch Animal Experimental Act and was approved by the Animal Experimental Committee of Maastricht University Medical Centre (DEC number 2014-120).

Materials

Alpha-cyano-4-hydroxycinnamic acid (CHCA), gelatin from porcine skin (type B) and trifluoroacetic acid (TFA) were purchased from Sigma-Aldrich (Gillingham, Dorset, UK). Methanol (MeOH) was purchased from Fisher Scientific (Loughborough, Leicestershire, UK). Norharmane (NOR) and chloroform ($CHCl_3$) were purchased from Sigma-Aldrich (Zwijndrecht, The Netherlands). Methanol, xylene and ethanol (EtOH) was purchased from Biosolve Valkenswaard, The Netherlands). Hematoxylin and eosin Y were purchased from Merck (Darmstadt, Germany) and J.T. Baker (Center Valley, PA, USA) respectively.

Tissue Preparation

A control mouse lung tissue was embedded in gelatin (100 mg/mL aqueous) and placed into a -80°C freezer[10]. Holes were drilled into the frozen gelatin using a RotaCraft RC12VS mini rotary tool kit (SHESTO Limited, Willesden, London, UK) fitted with a 3 mm diameter drill bit. The holes were then filled with control rat lung homogenate, which was prepared by adding 500 mg of tissue to a 2 mL tube that contained approximately 50 glass beads. The tube was then shaken at 4800 rpm for 3 × 60 secs using a mini-beadbeater (Biospec Products, Bartlesville, OK, USA). 200 µL of water was added to enable the homogenate to be pipetted into the holes in the gelatin block, which was stored on dry ice to immediately freeze the homogenate. These act as registration markers for later image reconstruction[12]. The embedded tissue was then sectioned at a temperature of -20°C using a Leica Cryostat (Leica, Wetzlar, Germany) to obtain 12 µm sections at 120 µm intervals, which were thaw mounted onto glass slides (Figure S1).

Matrix Application

The mice lung tissue sections were coated with 5 mg/mL CHCA in 70:30 MeOH: H_2O with 0.2% TFA was applied using a Suncollect automated pneumatic sprayer (Sunchrom, Friedrichsdorf, Germany) in a series of layers. The initial seeding layer was applied at 2 µL/minute and subsequent layers were performed at 3 µL/minute. The rat lung tissue sections were coated with 7 mg/mL NOR in 2:1 $CHCl_3$: MeOH using the HTX TM-sprayer (HTX technologies, Carrboro, NC, USA). The following settings were used temperature 30°C, flow rate 0.120 mL/min, velocity 1200 mm/min.

Instrumentation

Mass spectra and imaging data of mouse lung tissue were acquired in positive ion mode on an Applied Biosystems/MDS Sciex hybrid quadrupole time-of-flight mass spectrometer (Q-Star Pulsar-*i*) with an orthogonal MALDI ion source (Applied Biosystems, Foster City, California, USA) and a high repetition neodymium-doped yttrium vanadate (Nd:YVO_4) laser (5 kHz) (Elforlight Ltd, Daventry, Northamptonshire, UK). Image acquisition was performed at a spatial resolution of 150 µm × 150 µm in "Raster Image" mode; images were generated using the freely available Novartis Biomap 3.7.5.5 software (www.maldi-msi.org).

Analysis of rat lung tissue was performed using a Bruker rapifleX MALDI Tissuetyper system (Bruker Daltonik GmbH, Bremen, Germany) equipped with a Nd:YAG laser (10 kHz). The instrument was operated in reflectron mode in the mass range of *m/z* 400-1000. The instrument was calibrated prior to analysis using red phosphorus clusters[17]. The laser power was 80% with an accumulation of 100 shots. Images of the whole tissue sections were acquired using a 50 × 50 µm raster (25 × 25 µm beam scan area). The images were generated using the FlexImaging version 5.0 software (Bruker Daltonik GmbH).

Confirmation analysis in the form of tandem mass spectrometry (MS/MS) measurements were performed on a Waters MALDI HDMS Synapt G2-Si mass spectrometer (Waters Corporation, Manchester, UK) equipped with an neodymium-doped yttrium aluminium garnet (Nd:YAG) laser (1 kHz). The laser power was 200 arbitrary units and the ions of interest were fragmented by collision induced dissociation (CID) in the trap cell with an isolation window of approximately 3 Da (defined by the quadrupole low and high mass resolution in the

instrument control software). High mass resolution measurements (100,000 at *m/z* 500) were performed using on a Bruker solariX Fourier transform ion cyclotron resonance (FTICR) mass spectrometer (Bruker Daltonik GmbH, Bremen, Germany) equipped with a 9.4 T superconducting magnet and Nd:YAG laser (2 kHz). The instrument was operated in positive ion mode in the mass range *m/z* 100-1000.

Data processing

Images of selected masses generated in BioMap 3.8.0.4 software (https://ms-imaging.org/wp/biomap/) were exported in the JPEG format (File → Export → Image). Images of selected masses generated in FlexImaging 5.0 software (Bruker Daltonik GmbH) were copied to the clipboard. Using Microsoft PowerPoint (or available image processing software) the images were aligned using the fiducial markers as a guide, the images were cropped to ensure they were all the same size and saved in the JPEG format.

Using Image J 1.46r software (http://rsbweb.nih.gov/ij/), the individual images of the airway or parenchyma were opened in order and stacked together (Image → Stacks → Images to Stack). For visualization and presentation purposes, two of each image was opened to double the amount of sections. The stacks were then saved in the TIFF format. Once the images stacks were generated, they were converted into a 3D model that can be freely manipulated (Plugins → 3D → 3D viewer). In the 3D viewer, a second stack was added (File → Add content → from file). The transparency of the parenchyma was adjusted in order to better view of the airways. To do this, the parenchyma stack was selected (Select → check the tick box for the parenchyma stack) and the transparency was adjusted to the desired value (Edit → attributes → change transparency). Movies showing 360° views of the two 3D models was recorded in the 3D viewer window (View → Record 360 deg rotation),

Mass spectral post-processing and recalibration was performed using mMass software[18].

Histological staining

Hematoxylin and eosin (H&E) staining was performed on a rat lung tissue section post imaging. Following analysis, the tissue section was immersed in 100% MeOH for 30 seconds to remove the matrix. The sample was then washed with a series of solutions (1 × 100% EtOH, 2 × 95% EtOH, 2 × 70% EtOH and deionised water for 2 minutes each). The sample was then stained with hematoxylin for 3 minutes and subsequently washed with running tap water for 3 minutes. The tissue section was then stained with eosin for 30 seconds and then washed again with running tap water for 3 minutes. After staining the sample was placed into 100% EtOH for 1 minute, following this the tissue section placed in xylene for 30 seconds. After drying at room temperature, glass coverslips were placed onto the stained tissue section using Entellen mounting medium. A Leica Aperio CS2 (Leica Biosystems Imaging, Vista, CA, USA) was then used to acquire images of the stained tissue section.

Results and Discussion

One of the challenges of 3D MALDI-MS imaging is that it requires the preparation of high-quality tissue sections. The frozen tissue sample is sliced into serial sections, tissue tearing, rolled-up edges and deformations

can make the correlation of consecutive images difficult[19]. The preparation of lung tissue sections is challenging due to fragile parenchyma, often resulting in badly damaged tissue sections. In order to overcome this lung tissue is often inflated with embedding media in order to produce high quality tissue sections for MALDI-MS imaging[20]. Gelatin was chosen to externally embed the control mouse lung tissue because it preserves the integrity and morphology of the tissue, also gelatin provides less mass spectral interference than optimal cutting temperature (OCT) embedding media usually used for cryosectioning[10,21].

Once the embedding and sectioning method had been optimised, the next step was to obtain the molecular profiles of the tissue sections and registration markers. The MALDI-MS spectra obtained from the control mouse lung tissue and registration markers are shown in Figure 1.

A region of interest was drawn on the control mouse lung tissue and on one of the registration markers; the corresponding peak list was exported in text format and imported into the freely available mMass software[18]. The mass spectra (obtained from the two regions) were displayed in pairs by flipping one of the spectra as shown in Figure 2. In the case of both regions there is an abundance of possible lipid fragments such as choline at *m/z* 104.07, lysophosphatidylcholine (LPC) at *m/z* 496.33 and phosphocholine at *m/z* 184.08, which is the most abundant peak in both regions. The MALDI-MS spectra also show the presence of possible intact phospholipids in the range of *m/z* 700-800, the most abundant species in this region at *m/z* 734.55 and *m/z* 756.56 were tentatively identified as phosphatidylcholines (PC). In order to confirm the identity of the lipids MS/MS and accurate mass measurements were performed. Annotated MS/MS spectra of the selected endogenous species are shown in the supporting information (Figure S2A-I). High mass resolution accurate mass measurements were also performed to further confirm the molecular identities, these data are shown in Table S1. The MS/MS spectra were compared to those in the literature and databases such as lipid maps (www.lipidmaps.org) or the ALEX123 lipid calculator (www.alex123.info)[22].

Proper lipid identification is important in order to better understand the changes in lipid expression associated with different diseases, however it is challenging due to the complex nature of biological tissues. Measurements performed with high resolution mass spectrometers (FTICR) can provide better mass accuracy (~1 ppm), which can the provide an elemental formula that enables more accurate lipid database searches. However, these measurements can only provide the sum composition of the fatty acids chains and cannot differentiate between isomers.

In order to provide more information, tandem mass spectrometry (MS/MS) measurements are performed. The most abundant information gathered from MS/MS measurements in positive ion mode is related to the headgroup of the lipids. In the case of phospholipids, the most common peak that observed is that of phosphocholine at *m/z* 184. However other information can confirm if the lipid is protonated, sodiated or potassiated by monitoring peaks related to the headgroup cyclic 1,2-phosphodiester of phospholipids at *m/z* 125, 147 or 163 respectively[23,24]. Other peaks at *m/z* 60, 86 and 104 representing trimethylamine, dehydrated choline and choline are also related to the phospholipid headgroup but are present regardless of the ion type.

Corresponding peaks related to the neutral loss of the trimethylamine (-59 Da), phosphocholine headgroup (-183 Da) and sodiated or potassiated phosphocholine (-205 and 221 Da respectively) are also observed (Figures S2F, G and H).

MS/MS measurements can also determine the identity of the two fatty acid chains present in the lipid molecule, which was demonstrated with the peak at *m/z* 734.54 (Figure S2F). Two peaks at *m/z* 478.31 and 496.31 were observed, which corresponds to the neutral loss of palmitic acid or 16:0 (-256 Da) and ketene (-238 Da). As only two peaks were observed, it was determined that this was the phosphatidylcholine [PC (16:0/16:0)+H]$^+$. However, in the case of lipids with different fatty acid chains, the position of the fatty acid chains (termed *sn*-1 and *sn*-2) and position of double bonds cannot be determined with high resolution or MS/MS measurements. Using techniques such as ozone-induced dissociation (OzID) coupled with mass spectrometry imaging, it is now possible to obtain this information. It has also been demonstrated that isomeric lipid species have distinct distributions in biological tissues[25,26].Following profiling, MALDI-MS imaging was performed on a consecutive tissue section (adjacent tissue sections collected in between those used in the 3D model) in order to determine the distribution of the observed molecular species. The MALDI-MS images of selected ions related to molecular species are displayed in Figure 2.

The MALDI-MS images (Figure 2) show the distribution of various endogenous species throughout the control mouse lung tissue. From these data it can be seen that choline at *m/z* 104.07 (Figure 2A) is localised in specific regions of the tissue section and phosphocholine at *m/z* 184.08 (Figure 2D) is distributed throughout the control mouse lung tissue section. Other species included LPC related peaks such as [LPC (16:0)+H–H_2O]$^+$ at *m/z* 478.32 (Figure 2F), [LPC (16:0)+H]$^+$ at *m/z* 496.33 (Figure 2G), as well as the sodium and potassium adduct at *m/z* 518.33 and 543.33 (Figures 2H and 2J respectively). The ions at *m/z* 734.55 and 756.56 were identified as [PC (32:0)+H]$^+$ and its sodium adduct [PC (32:0)+Na]$^+$ (Figures 2K and 2L respectively). These species have been previously identified to be molecular markers for the parenchyma of the lung[27]. The images obtained, show that these species are also widespread throughout the lung tissue sections. Interestingly, the distribution of the selected molecular species appear to be influenced by the type of ion (protonated or cationized). This is observed in the images of protonated species (Figure 2B, D, F, G, I and K), which appear to be homogenously distributed throughout the lung tissue section. In contrast, sodiated and potassiated species (Figure A, C, E, H, J and K) are more localized in the parenchyma. All of the selected species were also observed in each of the homogenate registration markers located in the four corners of the images.

The generation of a three-dimensional image was performed by serially sectioning the mouse lung tissue with defined and measured spatial intervals (z-dimension), a total of 16 sections were collected and analyzed by MALDI-MSI. Phosphocholine at *m/z* 184.08, which was the most abundant lipid species, was chosen to show the structure of the lung tissue. The resulting 2D MALDI-MS images of the sixteen images generated showing the distribution of phosphocholine in the control mouse lung tissue are presented in Figure 3.

The 3D reconstruction of the distribution of phosphocholine at *m/z* 184.08 generated using the Image J software is shown in Figure 4 and is displayed from different angles.

The 3D MALDI-MS images showing the distribution of phosphocholine at *m/z* 184.08 (Figure 4) is displayed from different angles. The images show that phosphocholine is widely distributed and only shows the external structure of the control mouse lungs, however the images clearly display trachea and the right and left lobes. Following the evaluation of the method, the left lung of a rat was prepared in the same manner as the previous sample and cut into 24 sections. Upon analysis two species that defined the parenchyma and airways were detected, which were identified as $[PC\ (32:1)+K]^+$ at *m/z* 770.51 and $[PC\ (36:4)+K]^+$ at *m/z* 820.52 respectively. The individual images of the two species are shown in Figures S3 and S4 respectively, also the localization of these species in relation to histological features is presented in Figure 5. The hematoxylin and eosin (H&E) stain of the last tissue section in the stack post imaging (Figure 5A) shows the presence of the airways with blood vessels in close proximity, which are surrounded by the parenchyma. The MALDI-MS image of the parenchyma marker (Figure 5B) shows this is homogenously distributed but is absent from the airways and blood vessels. In contrast, the airway marker (Figure 5C) is located in the parenchyma but is elevated in the airway walls. The overlay (Figure 5D) clearly demonstrates the complementarity of these two species.

Previously identified species related to both the airways and parenchyma were also present in the data sets but were not used for the construction of the 3D models[27]. The 3D MALDI-MS images of the parenchyma and airway markers are shown in Figure 6.

The 3D MALDI-MS images (Figure 6) were constructed following alignment and viewed from different angles. The 3D MALDI-MS images of the parenchyma (Figure 6A) defines the shape of the lung. The 3D MALDI-MS image of the airways (Figure 6B) shows the presence of the large airways that further divide into smaller airways towards the periphery of the lungs. The overlay of the two 3D models (Figure 6C) shows the airways embedded within the parenchyma and further demonstrates how complementary the selected endogenous species are together (see videos 1-3 in the supporting information). Both species were also present in the fiducial markers around the tissue, however as observed in Figures S2 and S3, the fiducial markers are absent in later sections. This is due to air bubbles that can form when adding the homogenate into the drilled holes, which when frozen results in broken or missing fiducial markers. Should this happen the individual images can be aligned using the optical image as a guide.

Conclusions

The work presented here describes a method for monitoring the three-dimensional distribution of endogenous species in the lungs of a mouse. Control mouse lung tissue was serially sectioned resulting in 16 tissue section obtained at defined intervals, these sections were individually analyzed. Later another 3D model was constructed using a control rat lung, which was prepared in the same manner. Here two molecular markers, identified as ($[PC (32:1)+K]^+$) and ($[PC (36:4)+K]^+$) that defined the parenchyma and airways respectively were used. The addition of registration markers enabled straightforward image alignment, then utilizing Image J software the individual MALDI-MS images which showed the distribution of a specific endogenous species were stacked together and viewed as a 3D image.

Whilst the serial sectioning method requires careful sample preparation and is time consuming, the methodology could potentially be used to monitor the distribution of inhaled drug formulas in the lungs or endogenous species associated with respiratory diseases. Quantitation of compounds in individual tissue sections could be performed using previously reported methods[29].

Acknowledgements

This work was supported by a MRC case studentship from GlaxoSmithKline.

References

1. Sakas G. Trends in medical imaging: from 2D to 3D. *Comput Graph.* 2002;26(4):577-587.

2. Antoch G, Bockisch A. Combined PET/MRI: a new dimension in whole-body oncology imaging? *Eur J Nucl Med Mol Imaging.* 2009;36(1):113-120.

3. Fletcher JS, Rabbani S, Henderson A, Lockyer NP, Vickerman JC. Three-dimensional mass spectral imaging of HeLa-M cells--sample preparation, data interpretation and visualisation. *Rapid Commun Mass Spectrom.* 2011;25(7):925-932.

4. Nemes P, Barton AA, Vertes A. Three-dimensional imaging of metabolites in tissues under ambient conditions by laser ablation electrospray ionization mass spectrometry. *Anal Chem.* 2009;81(16):6668-6675.

5. Crecelius AC, Cornett DS, Caprioli RM, Williams B, Dawant BM, Bodenheimer B. Three-dimensional visualization of protein expression in mouse brain structures using imaging mass spectrometry. *J Am Soc Mass Spectrom.* 2005;16(7):1093-1099.

6. Andersson M, Groseclose MR, Deutch AY, Caprioli RM. Imaging mass spectrometry of proteins and peptides: 3D volume reconstruction. *Nat Methods.* 2008;5(1):101-108.

7. Sinha TK, Khatib-Shahidi S, Yankeelov TE, et al. Integrating spatially resolved three-dimensional MALDI IMS with in vivo magnetic resonance imaging. *Nat Methods.* 2008;5(1):57-59.

8. Mallah K, Quanico J, Trede D, et al. Lipid Changes Associated with Traumatic Brain Injury Revealed by 3D MALDI-MSI. *Anal Chem.* 2018;90(17):10568-10576.

9. Paine MRL, Liu J, Huang D, et al. Three-Dimensional Mass Spectrometry Imaging Identifies Lipid Markers of Medulloblastoma Metastasis. *Sci Rep.* 2019;9(1):2205-2205.

10. Chen R, Hui L, Sturm RM, Li L. Three dimensional mapping of neuropeptides and lipids in crustacean brain by mass spectral imaging. *J Am Soc Mass Spectrom.* 2009;20(6):1068-1077.
11. Eberlin LS, Ifa DR, Wu C, Cooks RG. Three-dimensional vizualization of mouse brain by lipid analysis using ambient ionization mass spectrometry. *Angew Chem Int Ed Engl.* 2010;49(5):873-876.
12. Chughtai K, Jiang L, Greenwood TR, et al. Fiducial markers for combined 3-dimensional mass spectrometric and optical tissue imaging. *Anal Chem.* 2012;84(4):1817-1823.
13. Vos DRN, Jansen I, Lucas M, et al. Strategies for managing multi-patient 3D mass spectrometry imaging data. *J Proteomics.* 2019;193:184-191.
14. Giordano S, Morosi L, Veglianese P, et al. 3D Mass Spectrometry Imaging Reveals a Very Heterogeneous Drug Distribution in Tumors. *Sci Rep.* 2016;6:37027.
15. Ogrinc Potocnik N, Porta T, Becker M, Heeren RM, Ellis SR. Use of advantageous, volatile matrices enabled by next-generation high-speed matrix-assisted laser desorption/ionization time-of-flight imaging employing a scanning laser beam. *Rapid Commun Mass Spectrom.* 2015;29(23):2195-2203.
16. Trede D, Schiffler S, Becker M, et al. Exploring three-dimensional matrix-assisted laser desorption/ionization imaging mass spectrometry data: three-dimensional spatial segmentation of mouse kidney. *Anal Chem.* 2012;84(14):6079-6087.
17. Sládková K, Houška J, Havel J. Laser desorption ionization of red phosphorus clusters and their use for mass calibration in time-of-flight mass spectrometry. *Rapid Commun Mass Spectrom.* 2009;23(19):3114-3118.
18. Strohalm M, Kavan D, Novak P, Volny M, Havlicek V. mMass 3: a cross-platform software environment for precise analysis of mass spectrometric data. *Anal Chem y.* 2010;82(11):4648-4651.
19. Chughtai K, Heeren RM. Mass spectrometric imaging for biomedical tissue analysis. *Chem Rev.* 2010;110(5):3237-3277.
20. Carter CL, Jones JW, Farese AM, MacVittie TJ, Kane MA. Inflation-Fixation Method for Lipidomic Mapping of Lung Biopsies by Matrix Assisted Laser Desorption/Ionization–Mass Spectrometry Imaging. *Anal Chem.* 2016;88(9):4788-4794.
21. Schwartz SA, Reyzer ML, Caprioli RM. Direct tissue analysis using matrix-assisted laser desorption/ionization mass spectrometry: practical aspects of sample preparation. *J Mass Spectrom.* 2003;38(7):699-708.
22. Pauling JK, Hermansson M, Hartler J, et al. Proposal for a common nomenclature for fragment ions in mass spectra of lipids. *PloS One.* 2017;12(11):e0188394.
23. Murphy RC, Hankin JA, Barkley RM. Imaging of lipid species by MALDI mass spectrometry. *J Lipid Res.* 2009;50 Suppl(Suppl):S317-322.
24. Berry KA, Hankin JA, Barkley RM, Spraggins JM, Caprioli RM, Murphy RC. MALDI imaging of lipid biochemistry in tissues by mass spectrometry. *Chem Rev.* 2011;111(10):6491-6512.
25. Ellis SR, Hughes JR, Mitchell TW, in het Panhuis M, Blanksby SJ. Using ambient ozone for assignment of double bond position in unsaturated lipids. *Analyst.* 2012;137(5):1100-1110.

26. Paine MRL, Poad BLJ, Eijkel GB, et al. Mass Spectrometry Imaging with Isomeric Resolution Enabled by Ozone-Induced Dissociation. *Angew Chem Int Ed Engl.* 2018;57(33):10530-10534.
27. Berry KA, Li B, Reynolds SD, et al. MALDI imaging MS of phospholipids in the mouse lung. *J Lipid Res.* 2011;52(8):1551-1560.
28. McDonnell LA, Römpp A, Balluff B, et al. Discussion point: reporting guidelines for mass spectrometry imaging. *Anal Bioanal Chem.* 2015;407(8):2035-2045.
29. Russo C, Brickelbank N, Duckett C, Mellor S, Rumbelow S, Clench MR. Quantitative Investigation of Terbinafine Hydrochloride Absorption into a Living Skin Equivalent Model by MALDI-MSI. *Anal Chem.* 2018;90(16):10031-10038.

Legends to Figures and Tables

Figure 1: MALDI-MS spectra obtained from the control mouse lung tissue (blue spectrum) and the registration markers (red spectrum). The annotated peaks were confirmed using MS/MS and high mass resolution measurements and later visualised.

Figure 2: MALDI-MS images showing the distribution of various endogenous species in the control mouse lung tissue section. A) choline at *m/z* 104.07, B) phosphocholine fragment at *m/z* 124.9, C) phosphocholine fragment at *m/z* 162.1, D) phosphocholine at *m/z* 184.08, E) $[LPA\ (18:1)+Na]^+$ at *m/z* 459.32, F) $[LPC\ (16:0)+H-H_2O]^+$ at *m/z* 478.32, G) $[LPC\ (16:0)+H]^+$ at *m/z* 496.32, H) $[LPC\ (16:0)+Na]^+$ at *m/z* 518.32, I) $[LPC\ (18:0)+H]^+$ at *m/z* 524.33, J) $[LPC\ (16:0)+K]^+$ at *m/z* 534.33, K) $[PC\ (16:0/16:0) + H]^+$ at *m/z* 734.55 and L) $[PC\ (16:0/16:0) + Na]^+$ at *m/z* 756.56. Spatial resolution 150 × 150 µm, normalized with protonated CHCA matrix peak at *m/z* 190.05.

Figure 3: 2D MALDI-MS images showing the distribution of phosphocholine at *m/z* 184.08 following normalization against the protonated CHCA matrix at *m/z* 190.05, throught the 16 control mouse lung tissue sections.

Figure 4: 3D MALDI-MS images produced using Image J software showing the distribution of phosphocholine at *m/z* 184.08 following normalization against the protonated CHCA matrix at *m/z* 190.05, throughout the control mouse lung tissue from different angles.

Figure 5: Correlation of molecular markers with histological staining. A) Hematoxylin and eosin (H&E) staining of lung tissue post imaging. MALDI-MS images showing the distribution of B) parenchyma marker ($[PC\ (32:1)+K]^+$) at *m/z* 770.51, C) airway marker ($[PC\ (36:4)+K]^+$) at *m/z* 820.52 and D) overlay of selected molecular markers. Spatial resolution 50 × 50 µm, normalized with TIC as indicated by the red "T" in the top right corner based on reporting nomenclature[28].

Figure 6: 3D MALDI-MS images of the parenchyma and airways. 3D MALDI-MS images showing the distribution of A) $[PC\ (32:1)+K]^+$ at *m/z* 770.51 that highlights the parenchyma and B) $[PC\ (36:4)+K]^+$ at *m/z* 820.52 that highlights the airways. C) Overlay of the parenchyma and airway 3D models (transparency of the parenchyma stack set to 12%).

Figure 1:

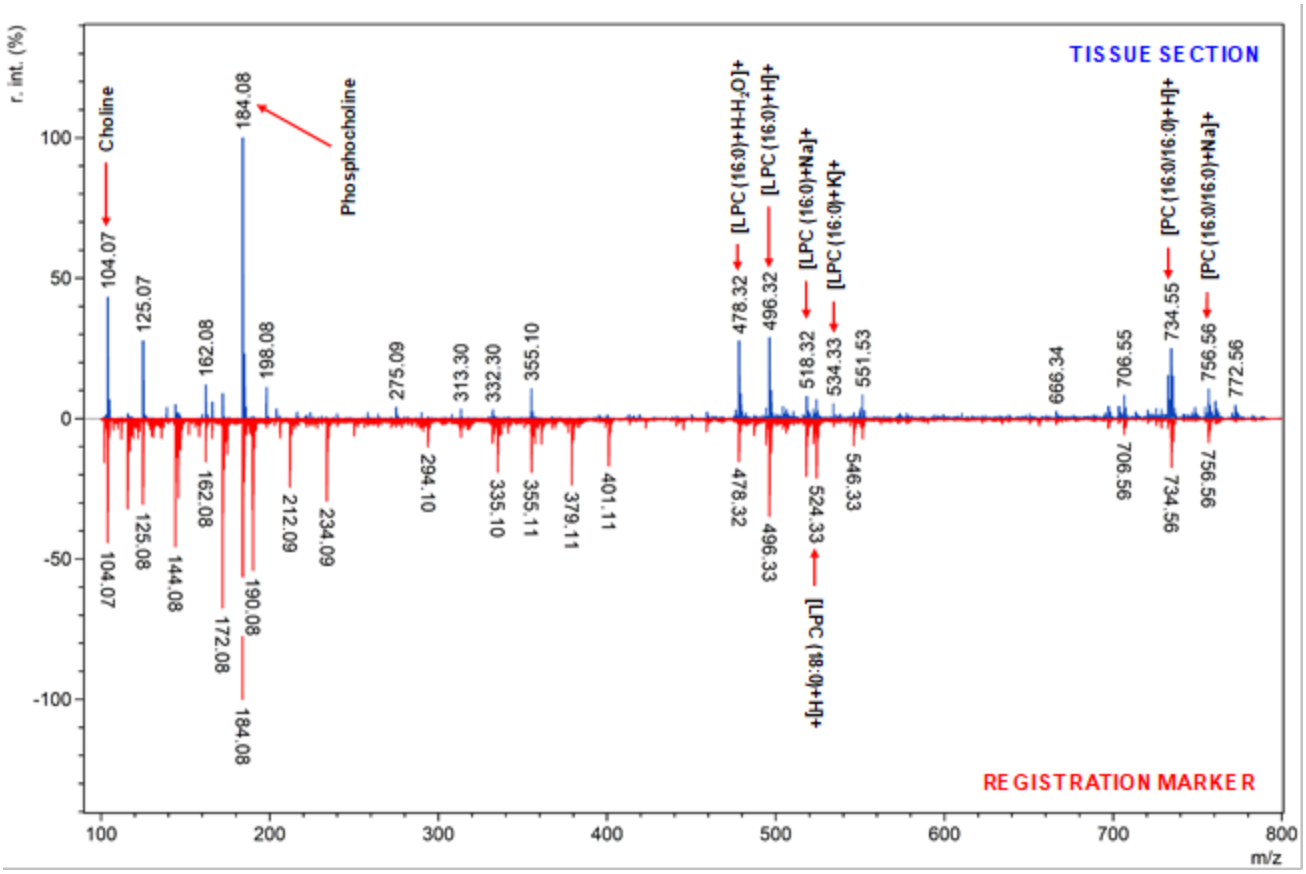
TISSUE SECTION
REGISTRATION MARKER
r. int. (%)
m/z
Choline
Phosphocholine
[LPC (16:0)+H-H2O]+
[LPC (16:0)+H]+
[LPC (16:0)+Na]+
[LPC (16:0)+K]+
[PC (16:0/16:0)+H]+
[PC (16:0/16:0)+Na]+
[LPC (18:0)+H]+
104.07
125.07
162.08
184.08
198.08
275.09
313.30
332.30
355.10
478.32
496.32
518.32
534.33
551.53
666.34
706.55
734.55
756.56
772.56
144.08
172.08
190.08
212.09
234.09
294.10
335.10
355.11
379.11
401.11
478.32
496.33
524.33
546.33
706.56
734.56
756.56

Figure 2

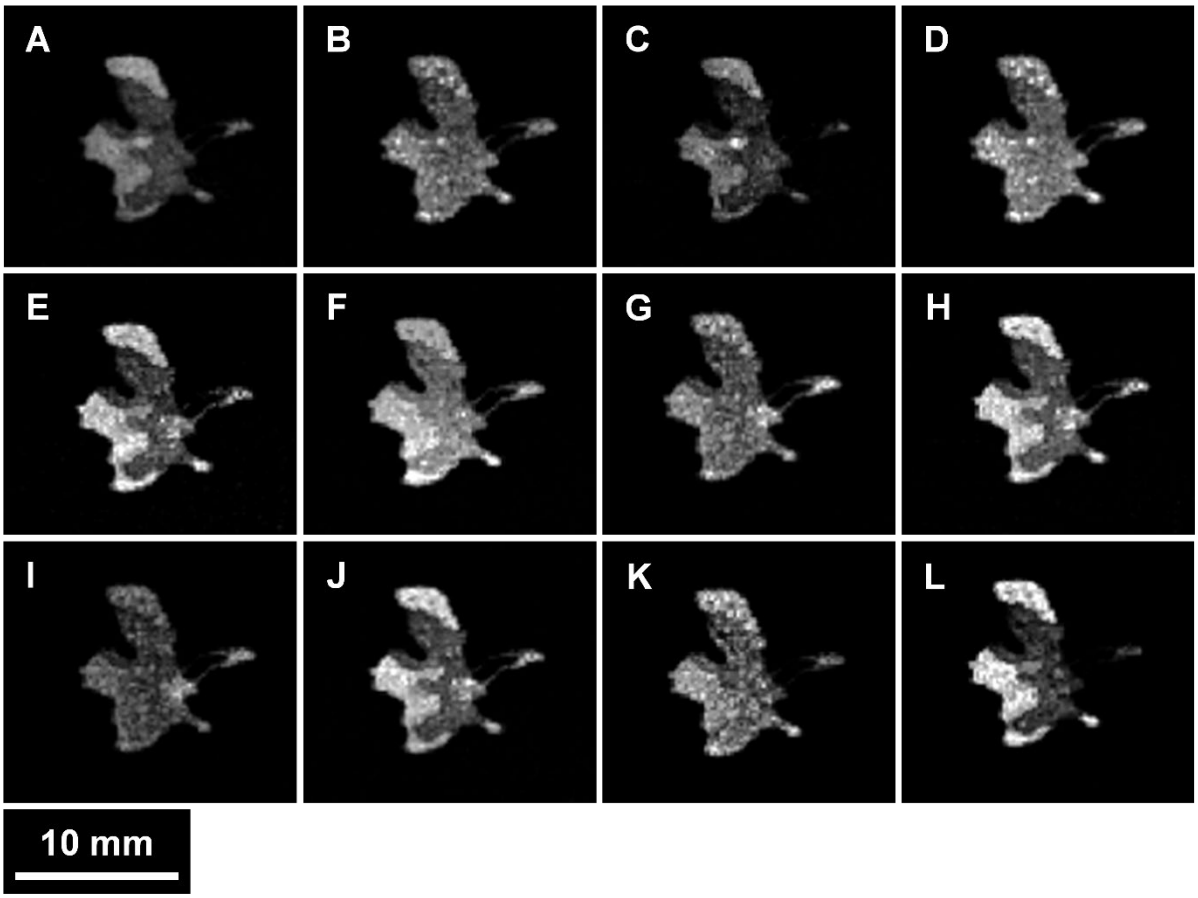

Figure 3

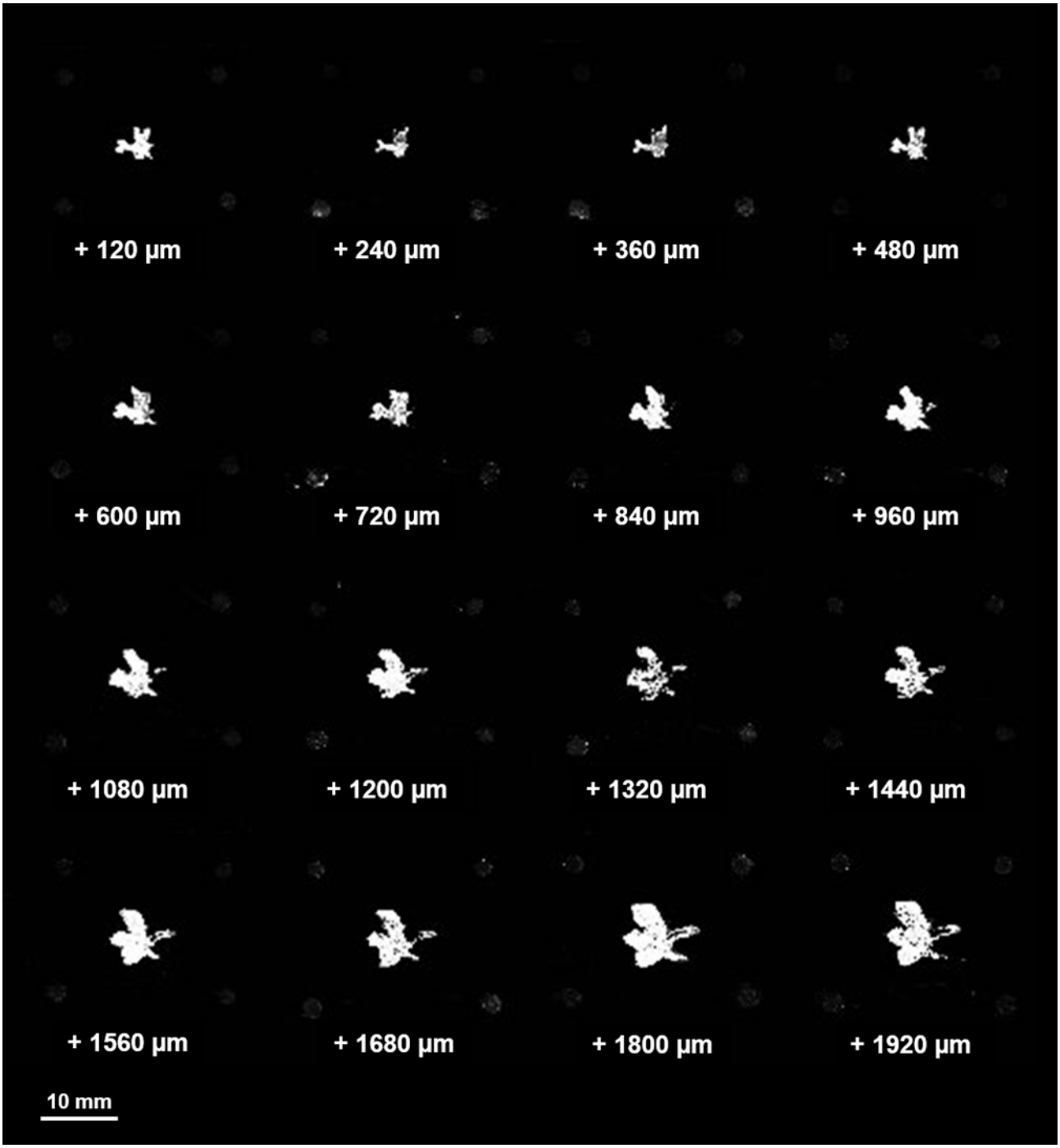
+ 120 µm
+ 240 µm
+ 360 µm
+ 480 µm
+ 600 µm
+ 720 µm
+ 840 µm
+ 960 µm
+ 1080 µm
+ 1200 µm
+ 1320 µm
+ 1440 µm
+ 1560 µm
+ 1680 µm
+ 1800 µm
+ 1920 µm
10 mm

Figure 4

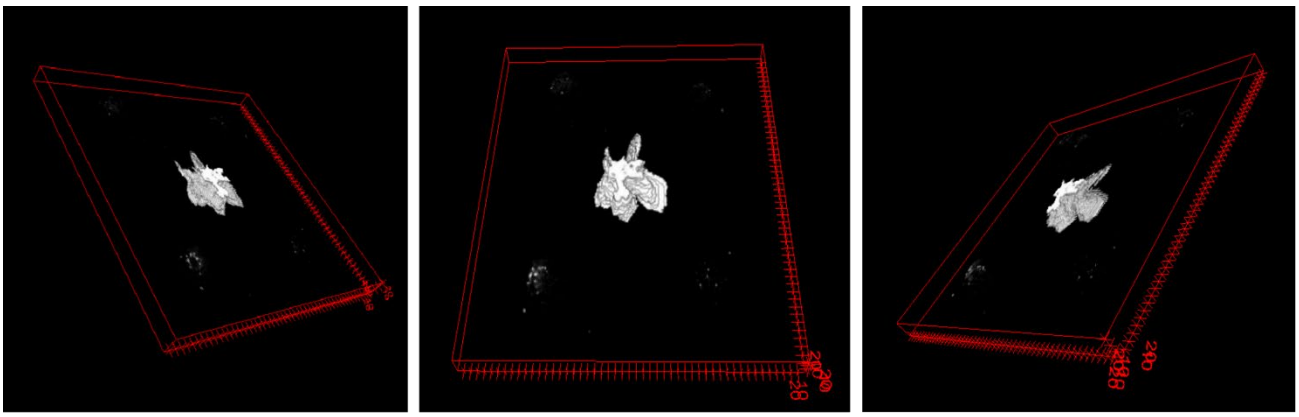

Figure 5

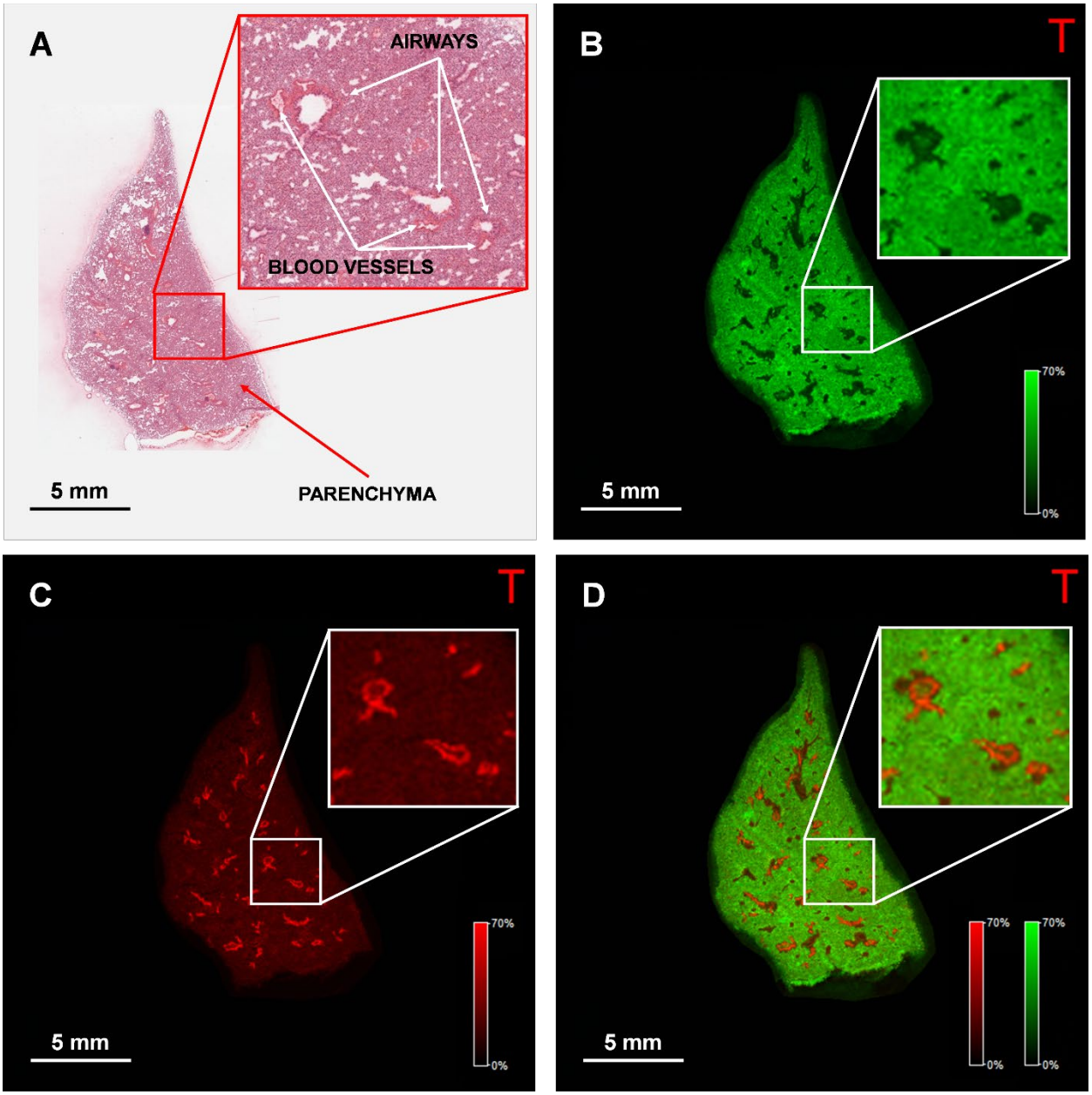
A
AIRWAYS
BLOOD VESSELS
PARENCHYMA
5 mm
B
T
70%
0%
5 mm
C
T
70%
0%
5 mm
D
T
70%
0%
70%
0%
5 mm

Figure 6